

Revealing the Electronic Structure of NiPS₃ through Synchrotron-Based ARPES and Alkali Metal Dosing

Yifeng Cao^{1, 4†}, Qishuo Tan^{2†}, Yucheng Guo^{3, 4†}, Clóvis Guerim Vieira⁶, Mário S. C. Mazzoni⁷, Jude Laverock⁵, Nicholas Russo¹, Hongze Gao², Chris Jozwiak⁴, Aaron Bostwick⁴, Eli Rotenberg⁴, Jinghua Guo⁴, Ming Yi³, Matheus J. S. Matos^{6*}, Xi Ling^{2, 8, 9*}, and Kevin E. Smith^{1, 2, 8*}

¹ Department of Physics, Boston University, Boston, Massachusetts, 02215, USA.

² Department of Chemistry, Boston University, Boston, Massachusetts, 02215, USA.

³ Department of Physics and Astronomy, Rice University, Houston, Texas, 77005, USA.

⁴ Advanced Light Source, Lawrence Berkeley National Laboratory, Berkeley, California, 94720, USA.

⁵ School of Chemistry, University of Bristol, Bristol, BS8 1QU, UK.

⁶ Departamento de Física, Universidade Federal de Ouro Preto, Ouro Preto, CEP 35400-000, Brazil.

⁷ Departamento de Física, Universidade Federal de Minas Gerais, Belo Horizonte, CEP 31270-901, Brazil.

⁸ Division of Materials Science and Engineering, Boston University, Boston, Massachusetts, 02215, USA.

⁹ The Photonics Center, Boston University, Boston, Massachusetts, 02215, USA.

†These authors contributed equally to this work.

*To whom the correspondence should be addressed. Email address: matheusmatos@ufop.edu.br; xiling@bu.edu; ksmith@bu.edu

Keywords: angle-resolved photoemission spectroscopy; density functional theory; alkali metal dosing; 2D magnetic materials; defect states

Abstract

This study presents a comprehensive analysis of the band structure in NiPS₃, a van der Waals layered antiferromagnet, utilizing high-resolution synchrotron-based angle-resolved photoemission spectroscopy (ARPES) and corroborative density functional theory (DFT) calculations. By tuning the parameters of the light source, we obtained a very clear and wide energy range band structure of NiPS₃. Comparison with DFT calculations allows for the identification of the orbital character of the observed bands. Our DFT calculations perfectly match the experimental results, and no adaptations were made to the calculations based on the experimental outcomes. The appearance of novel electronic structure upon alkali metal dosing (AMD) were also obtained in this ARPES study. Above valence band maximum, structure of conduction bands and bands from defect states were firstly observed in NiPS₃. We provide the direct determination of the band gap of NiPS₃ as 1.3 eV from the band structure by AMD. In addition, detailed temperature dependent ARPES spectra were obtained across a range that spans both below and above the Néel transition temperature of NiPS₃. We found that the paramagnetic and antiferromagnetic states have almost identical spectra, indicating the highly localized nature of Ni *d* states.

Introduction

Van der Waals (vdW) layered materials, such as metal phosphorus trichalcogenides MPX₃ (M=Ni, Mn, Fe, etc. and X=S, Se) are important two-dimensional crystals. Their unique intercalation-substitution or intercalation-reduction behaviour and the incipient ionic conductivity, allow them to be applied in Li-ion batteries¹, hydrogen storage², and photo-electrochemical reactions³. Of the various MPX₃ materials, we focus here on NiPS₃ which is an zigzag-type antiferromagnet [see Fig. 1(a)] with a Néel transition temperature (T_N) at 155 K⁴. NiPS₃ exhibits intriguing properties in electronics^{5,6}, spintronics⁷⁻⁹, magnetism¹⁰⁻¹³, and optics^{14,15}. The most unusual property of NiPS₃ is its ultrasharp photoluminescence (PL) peak, induced by a spin-orbit-entangled exciton state, which originates from intrinsically many-body localized states in the form of a Zhang-Rice singlet, appearing below T_N ¹⁶. This exciton state has been widely studied¹⁷⁻²⁰, highlighting the importance of researching the electronic structure of NiPS₃, including both the valence bands (VB) and the conduction bands (CB).

Angle-resolved photoemission spectroscopy (ARPES) allows for the direct measurement of the electronic structure of the occupied VB. With alkali metal dosing (AMD), charge will transfer from the alkali metal to the surface of the material²¹⁻²³, potentially resulting in the emergence of novel electronic states in a dosed sample²⁴⁻²⁶, making ARPES even capable of probing the unoccupied CB. To thoroughly explore the comprehensive electronic structure of NiPS₃, the ARPES method is undoubtedly necessary.

Recently, several studies have utilized lab-based ARPES to investigate the electronic structure of NiPS₃ single crystals^{19,27}, as well as other MPX₃ materials, including MnPS₃²⁸, CoPS₃²⁹ and FePS₃²⁷. However, although a small number of bands were observed, the majority of bands are either fuzzy or even invisible due to the limited resolving power of lab-based ARPES and the relative large band gap of NiPS₃ (ranging from 1.4 eV to 1.8 eV, including both direct and indirect bandgaps^{5,18,30,31}, reported by different studies). Moreover, density functional theory (DFT) calculations are commonly used to elucidate ARPES experimental results; however, for NiPS₃, current DFT calculations do not align well with experimental findings¹⁹. Several renormalizations with rigid energy shifts are needed to match the calculated bands with the actual ARPES data, which naturally diminishes the soundness of the interpretation by DFT. The

above indicates that there has been a lack of comprehensive ARPES studies and corresponding theoretical calculations for NiPS₃ until now.

Here, we present a comprehensive synchrotron-based ARPES study on NiPS₃. The NiPS₃ sample was exfoliated into nanoscale flakes, enhancing the conductivity and thus yielding stronger ARPES signals. By tuning the photon source, a very clear band structure was obtained, even capturing deep bands at energy relative to the valence band maximum (VBM) ($E - E_{VBM}$) down to -7.3 eV. Further, we applied AMD on the surface NiPS₃ flakes at low temperature to probe the bands above VBM. Consequently, both the CB and band from defect states were observed after dosing. Then the band gap of NiPS₃ was directly obtained from the band structure. The ARPES data were compared to a theoretical calculation using DFT+U to help us better understand the electronic structure of NiPS₃ by determining the relative contribution of each element pair to the obtained band structure. Our calculations align exceptionally well with the experimental results in both VB and CB, and we did not make any artificial adjustments to the calculations based on the experimental data. Moreover, temperature-dependent ARPES measurements were applied to NiPS₃ across its T_N . Unlike an apparent band splitting in MnPS₃ when across T_N ²⁸, NiPS₃ shows very identical ARPES spectra in both paramagnetic and antiferromagnetic states, which revealed its well-localized Ni d states.

Methods

NiPS₃ sample preparation. Pure elements, in a stoichiometric ratio of Ni:P:S = 1:1:3 (2 g in total), along with 40 mg iodine as transport agent, were enclosed in quartz ampules under vacuum of 1×10^{-4} Torr. Subsequently, the ampules underwent heating in a two-zone furnace with the temperature range of 650 – 600 °C for 1 week, followed by cooling to room temperature. Bulk crystals were harvested from the lower temperature zone of the ampules. Thin flakes were acquired through mechanical exfoliation on boron-doped Si substrates (coated with 1nm/5nm titanium/gold film to enhance the flake adhesion [see Fig 1(c)]) using scotch-tape, and their thicknesses were determined by atomic force microscopy (Bruker Dimension 3000). Many flakes are on the same substrate. We selected target samples with a thickness of approximately 10-50 nm and an area with a uniform thickness greater than $20 \times 20 \mu\text{m}$.

ARPES setup. We probed the NiPS₃ with μ -ARPES at Advanced Light Source beamline 7.0.2 at Lawrence Berkeley National Laboratory. The μ -ARPES has spot size less than $10 \mu\text{m}$ and energy resolution down to 16 meV. Prior to μ -ARPES measurements, the samples were transferred to the preparation chamber and annealed at 350°C for 12 hours. The photon energy in μ -ARPES was tunable and we covered the range from 63 eV to 153 eV. The experiment revealed that the photon energy of 126 eV with linear horizontal (LH) polarization provides the clearest band structure for NiPS₃ [see Fig 1(c)]. AMD was performed by depositing potassium onto the surface of a NiPS₃ flake at 7 K. A well-outgassed potassium getter source, operated at a current of 7 A, was used for dosing, with each round lasting for 1 minute. To obtain the spectra across the T_N (155 K) of NiPS₃, the temperature range of our experiments span from 6 K to 182 K.

Computational methods To elucidate the band structure of NiPS₃, we perform ab initio calculations based on the density functional theory with on-site Coulomb correlations (DFT+U)³²⁻³⁴. The calculations were performed utilizing the VASP code using the projector-augmented wave³⁵⁻³⁹. To account for the on-site Coulomb repulsion between the 3d electrons of Ni ions, we adopt the GGA+U formalism proposed by Dudarev³⁴, with effective Hubbard U parameters ranging from 1 eV to 5 eV, in conjunction with the Perdew-Burke-Ernzerhof (PBE) exchange-correlation

functional⁴⁰. Band structure plotting was conducted utilizing band unfolding techniques as implemented in the VASP software⁴¹, facilitating direct comparison with ARPES experimental data. We compare DFT+U electronic band positions with ARPES data to determine the optimal U parameter for pristine and K-adsorbed NiPS₃. The plane-wave basis set employed in the calculations utilized an energy cutoff of 515 eV and the criteria for energy convergence was set to 10⁻⁵ eV. Geometries were optimized until the maximum atomic force was below 10 meV/Å. We simulate the zigzag antiferromagnetic configuration in NiPS₃ employing a 2x2x1 supercell for bulk calculations and 2x2 supercells for both monolayer and bilayer structures. To achieve geometric relaxation of the structures, a Gamma-centered k-grid of 6x6x1 was employed. To accurately describe Van der Waals interactions between layers, we used the DFT-D3 method of Grimme with zero-damping⁴². The density of states (DOS) analysis was performed using VASP software⁴¹.

Results

To obtain a clear ARPES signal from an insulator, we exfoliated NiPS₃ into nanoscale flakes to reduce the charging effect. On the other hand, we found that flakes that are too thin (below about 5 layers) will have insufficient sample strength, resulting in poor surface flatness, making it difficult to observe dispersive states. Empirically, samples with a thickness of 10-50 nm yield the best ARPES signals. The detailed band structure of NiPS₃ along $\overline{MK\Gamma KM}$ direction is presented in Fig. 2(a), with white arrows indicate the position of the bands. As an insulator, NiPS₃ does not have a well-defined Fermi level. Here the E_{VBM} is defined as the position of the kink feature in the energy distribution curve (EDC) curve. The corresponding projected surface BZ is displayed in Fig. 1(b), with $\overline{KT\bar{K}}$ region in the first BZ and \overline{M} points from second BZ. To identify the orbital contributions to the measured band structure, we compared the ARPES data with the band structure calculated from DFT+U [see Fig. 2(b)-(d)]. For simplicity, we only show the atomic orbitals that primarily contribute to the bands indicated by white arrows in Fig. 2(a), including the $d_{x^2-y^2}$ and d_{z^2} orbitals of Ni (red), and the p_z orbitals of S (green) and P (blue). Excellent agreement was achieved between the ARPES data and DFT+U calculations without any rigid energy shifts or renormalizations, allowing for the assignment of the primary contribution of atomic orbitals to each band.

The band closest to E_{VBM} is primarily due to Ni and S states, and exhibits pronounced asymmetry, with a strong intensity near the left K point. This can also be seen from the constant energy map at E_{VBM} in Fig. 2(e), where the hexagonal pocket in the center exhibits strong intensities only for the \overline{K} points at the alternating corners of the hexagon. A very distinct flat band with strongest intensity contributed by Ni d states appears at $E - E_{VBM} = -1$ eV. The flatness of this band corroborates the model wherein the Ni d states form highly localized levels within board bands formed by the P₂S₆ lattice⁴³. In the energy range from -2 eV to -6 eV, several bands are observed. These bands are primarily composed of hybridized states of Ni d states and S p states. The contribution of P p states is primarily in a very deep energy range: a hybridized state of P and S can be observed near $E - E_{VBM}$ of -7.3 eV. Fig. 2(e)-(h) present the constant energy maps at different energies ($E - E_{VBM}$). The threefold symmetry of the VB can be clearly observed from constant energy maps with varying sizes of hexagonal pockets at different $E - E_{VBM}$ around the $\overline{\Gamma}$ point.

The ARPES data for potassium dosing results are presented in Fig. 3(a)-(c). During the AMD process, the charge transferred from K atoms to the surface of NiPS₃. The transferred electrons will enter the unoccupied CB, resulting in the entire electronic band structure of NiPS₃ being

pushed upward in energy. Here the energy of spectra after dosing were calibrated by the features in the VB from the pristine sample. We found that the features in the VB remain unchanged throughout the entire dosing process, except for becoming blurred due to the increased coverage of K atoms on the sample surface with additional dosing rounds. In contrast, two new bands appear above the original E_{VBM} (images on the upper part of Fig. 3(a)-(c)) at approximately 0.7 eV and 1.3 eV after dosing, as labeled by the red and orange arrows. The above observations can also be derived from the EDC in Fig. 3(d): the positions of the bands in the VB remain unchanged, while their intensity decreases with increasing dosing sequence; in the CB, two new peaks appear at the positions indicated by the red and orange arrows as dosing progresses. Further examination of the details of these two newly appeared bands reveals that the band at 0.7 eV is very flat and extends across the entire BZ, while the band at 1.3 eV has higher intensity and broader bandwidth around the \bar{K} point.

To elucidate the newly appeared ARPES features above E_{VBM} , the DFT+U calculation for the CB is presented in Fig. 3(e)-(g), including the pristine NiPS₃ and NiPS₃ combined with K atoms. For the pristine NiPS₃ [Fig. 3(e)], the calculated lowest CB labeled with orange arrow appears around 1.3 eV, which matches with the ARPES data in dosed sample. For the calculation with NiPS₃ combined with one K atom per site [Fig. 3(f)], more bands appear, but the features in the VB and the position of the lowest CB remain largely unchanged. Moreover, the DFT calculation indicate the lowest CB also has broader bandwidth around the \bar{K} point. This is in excellent agreement with what we observed in both the VB and CB regions during our dosing experiments. In addition, the atomic orbital analysis found that the band labeled by the orange arrow is contributed by Ni and S, with no contribution from K atoms, strongly proving that this band belongs to the lowest CB of NiPS₃. Therefore, we directly obtained the band gap of NiPS₃ from the band structure as 1.3 eV, which is smaller than the band gaps of NiPS₃ reported in previous studies^{5,18,30,31}.

The remaining question is the origin of the flat band appearing around 0.7 eV indicated by the red arrow. Compared to the lowest conduction band at 1.3 eV, the 0.7 eV band is flatter and appears within the band gap, making it very likely to originate from localized defect states⁴⁴. Compared with a perfect crystal, where the electronic states are delocalized across the lattice due to the uniform potential, defects create localized disruptions in this potential, causing the electronic states associated with these defects to also become localized. In addition, the defect states represent altered electron configurations, which often do not match the energies of the delocalized states in the perfect crystal, resulting in energies that lie within the band gap. NiPS₃ has been found to have natural or engineered vacancies of S or Ni elements^{45,46}. Related calculations also indicate that the absence of S in NiPS₃ will lead to the formation of defect states within the band gap⁴⁷. During the AMD process, the introduction of K atoms can also make the NiPS₃ sample surface more prone to defect states, leading to the formation of the flat band at 0.7 eV within the band gap.

Fig. 3(g) presents another calculation model where NiPS₃ combined with two K atoms per site. Consequently, more bands appear above the E_{VBM} , which could potentially be an alternative origin of the newly appeared band at around 0.7 eV. However, this contradicts the phenomena observed in our experiments. From the two K atoms model, it is evident that the features of the valence band change significantly compared to the pristine sample, and the lowest CB splits into two bands. However, in the experiment, as the dosing rounds increase, the newly appeared band does not split. This can also be seen from the core level spectra in Fig. 3(h), where the K 3p peak does not split during the dosing, indicating that there is no transition from a one K atom model to a two K atoms model in our AMD experiment.

Thus far, all the experiments report here have been conducted at a temperature of around 6

K, which is within the antiferromagnetic state of NiPS₃. We next investigated whether the band structure changes when NiPS₃ is heated above T_N (155 K). Fig. 4(a) shows the ARPES data of NiPS₃ in its paramagnetic state at 182 K. Surprisingly, although the increased thermal motion of molecules due to the temperature rise results in slightly blurred band structures and a slight upward shift in the overall image due to the charging effect in Fig. 4(a) compared to the ARPES data at 6 K, the band structures observed at 182 K are almost identical. The entire temperature ramping process can be seen in Fig. 4(b), where the positions and intensities of all the peaks show no significant changes. Fig. 4(c)-(e) show the detailed changes during temperature ramping of the strongest peak observed near -1 eV in ARPES (flat band contributed by Ni), as indicated by the blue arrows in Fig. 4(b). Above T_N (dashed line), the peak intensity shows an obvious drop [Fig. 4(d)]. As the temperature increases, the shape of the band also changes slightly [Fig. 4(c)], but the FWHM analysis shows no trend changes on either side of T_N [Fig. 4(e)]. Therefore, the ARPES spectra of NiPS₃ largely remain unchanged when crossing T_N . This is entirely different from the case of MnPS₃. Jeff *et al.*²⁸ found that when MnPS₃ transfer from the paramagnetic state to the antiferromagnetic state, there is a clear splitting of the Mn 3*d* bands around the Γ point, accompanied by some subtle changes in S 3*p* bands. Such significant changes in band structure across T_N are very likely to be diminished by the well-localized Ni 3*d* states, as observed in both this study and other research⁵.

Conclusions

In summary, we have successfully measured the band structure of NiPS₃ for both the VB and the CB utilizing synchrotron-based ARPES, and compared our measurements to original DFT+U calculations. By optimizing the ARPES setup, the band structure of NiPS₃ from $E - E_{VBM} = 0$ eV down to -7.3 eV was clearly observed. Moreover, for the first time, excellent agreement was achieved between the theoretical DFT+U calculations and the ARPES data without any shifting or renormalization to adapt to the experimental results. Moreover, the atomic orbital to which each band belongs was also determined by DFT calculations. By dosing with potassium, new electronic states emerged in NiPS₃, revealing both the electronic structure of CB and bands from defect states. From the AMD process, the band gap was directly determined from the band structure, with a value of 1.3 eV. In addition, the temperature-dependent measurements revealed that, unlike MnPS₃, the band structure of NiPS₃ in the antiferromagnetic state (below T_N) and the paramagnetic state (above T_N) is nearly identical, due to the highly localized Ni *d* orbitals. Our study not only advances the understanding of NiPS₃'s electronic landscape but also demonstrates the power of integrating ARPES with theoretical methods to explore and manipulate the electronic structures of complex materials.

Data availability. Data that support the study in this article are available from the corresponding authors on reasonable request.

Acknowledgements. This research used resources of the Advanced Light Source, which is a Department of Energy (DOE) Office of Science User Facility under contract no. DE-AC02-05CH11231. Q.T. acknowledges the support by the National Science Foundation (NSF) under Grant No. 1945364. X.L. acknowledges the membership of the Photonics Center at Boston University. M.J.S.M, C.G.V, and M.S.C.M formally acknowledge the financial support provided by CNPq, CAPES, FAPEMIG, the Brazilian Institute of Science and Technology (INCT) in Carbon Nanomaterials, and Rede Mineira de Materiais 2D (FAPEMIG). The authors are also grateful to the National Laboratory for Scientific Computing (LNCC/MCTI, Brazil) in São Paulo (CENAPAD-SP) and the SDumont supercomputer in Rio de Janeiro for their invaluable assistance. Furthermore, M.J.S.M, C.G.V, and M.S.C.M express appreciation for the postdoctoral scholarship funded by project CNPq-405910/2022-3. M.J.S.M additionally acknowledges the financial support extended by Universidade Federal de Ouro Preto (UFOP).

Competing interests. The authors declare no competing interests.

References

- [1] Kuzminskii, Y. V., Voronin, B. & Redin, N. Iron and nickel phosphorus trisulfides as electroactive materials for primary lithium batteries. *Journal of power sources* **55**, 133–141 (1995).
- [2] Ismail, N., Madian, M. & El-Meligi, A. Synthesis of nips₃ and cops and its hydrogen storage capacity. *Journal of alloys and compounds* **588**, 573–577 (2014).
- [3] Byvik, C. E., Smith, B. T. & Reichman, B. Layered transition metal thiophosphates (mpx₃) as photoelectrodes in photoelectrochemical cells. *Solar Energy Materials* **7**, 213–223 (1982).
- [4] Le Flem, G., Brec, R., Ouyard, G., Louisy, A. & Segransan, P. Magnetic interactions in the layer compounds mpx₃ (m= mn, fe, ni; x= s, se). *Journal of Physics and Chemistry of Solids* **43**, 455–461 (1982).
- [5] Kim, S. Y. *et al.* Charge-spin correlation in van der waals antiferromagnet nips₃. *Physical review letters* **120**, 136402 (2018).
- [6] Tan, Q. *et al.* Charge-transfer-enhanced d–d emission in antiferromagnetic nips₃. *Applied Physics Reviews* **9** (2022).
- [7] Wang, X. *et al.* Spin-induced linear polarization of photoluminescence in antiferromagnetic van der waals crystals. *Nature Materials* **20**, 964–970 (2021).
- [8] Basnet, R., Wegner, A., Pandey, K., Storment, S. & Hu, J. Highly sensitive spin-flop transition in antiferromagnetic van der waals material m p s₃ (m= ni and mn). *Physical Review Materials* **5**, 064413 (2021).
- [9] Scheie, A. *et al.* Spin wave hamiltonian and anomalous scattering in nips₃. *Physical Review B* **108**, 104402 (2023).
- [10] Wildes, A. R. *et al.* Magnetic structure of the quasi-two-dimensional antiferromagnet nips₃. *Physical Review B* **92**, 224408 (2015).
- [11] Kim, K. *et al.* Suppression of magnetic ordering in xxz-type antiferromagnetic monolayer nips₃. *Nature communications* **10**, 345 (2019).
- [12] He, W. *et al.* Magnetically propagating hund’s exciton in van der waals antiferromagnet nips₃. *Bulletin of the American Physical Society* (2024).
- [13] Tan, Q. & Furthmüller, J. Observation of three-state nematicity and domain evolution in atomically thin antiferromagnetic nips₃. *Nano Lett.* **24**, 7166–7172 (2024). URL <https://pubs.acs.org/doi/abs/10.1021/acs.nanolett.4c00772>.
- [14] Liu, J. *et al.* Nips₃ nanoflakes: a nonlinear optical material for ultrafast photonics. *Nanoscale* **11**, 14383–14391 (2019).
- [15] Wang, X. *et al.* Electronic raman scattering in the 2d antiferromagnet nips₃. *Science Advances* **8**, eabl7707 (2022).
- [16] Kang, S. *et al.* Coherent many-body exciton in van der waals antiferromagnet nips₃. *Nature* **583**, 785–789 (2020).

- [17] Belvin, C. A. *et al.* Exciton-driven antiferromagnetic metal in a correlated van der waals insulator. *Nature communications* **12**, 4837 (2021).
- [18] Ho, C.-H., Hsu, T.-Y. & Muhimmah, L. C. The band-edge excitons observed in few-layer nips3. *npj 2D Materials and Applications* **5**, 8 (2021).
- [19] Klaproth, T. *et al.* Origin of the magnetic exciton in the van der waals antiferromagnet nips 3. *Physical Review Letters* **131**, 256504 (2023).
- [20] Kim, D. S. *et al.* Anisotropic excitons reveal local spin chain directions in a van der waals antiferromagnet. *Advanced Materials* **35**, 2206585 (2023).
- [21] Muscat, J. & Batra, I. P. Coverage dependence of the work function of metals upon alkali-metal adsorption. *Physical Review B* **34**, 2889 (1986).
- [22] Aruga, T. & Murata, Y. Alkali-metal adsorption on metals. *Progress in surface science* **31**, 61–130 (1989).
- [23] Diehl, R. & McGrath, R. Current progress in understanding alkali metal adsorption on metal surfaces. *Journal of Physics: Condensed Matter* **9**, 951 (1997).
- [24] Ohta, T., Bostwick, A., Seyller, T., Horn, K. & Rotenberg, E. Controlling the electronic structure of bilayer graphene. *Science* **313**, 951–954 (2006).
- [25] Zhang, Y. *et al.* Direct observation of the transition from indirect to direct bandgap in atomically thin epitaxial mose2. *Nature nanotechnology* **9**, 111–115 (2014).
- [26] Kim, J. *et al.* Observation of tunable band gap and anisotropic dirac semimetal state in black phosphorus. *Science* **349**, 723–726 (2015).
- [27] Yan, M., Jin, Y., Voloshina, E. & Dedkov, Y. Electronic correlations in fe x ni y ps3 van der waals materials: Insights from angle-resolved photoelectron spectroscopy and dft. *The Journal of Physical Chemistry Letters* **14**, 9774–9779 (2023).
- [28] Strasdas, J. *et al.* Electronic band structure changes across the antiferromagnetic phase transition of exfoliated mnps3 flakes probed by μ -arpes. *Nano Letters* **23**, 10342–10349 (2023).
- [29] Voloshina, E., Jin, Y. & Dedkov, Y. Arpes studies of the ground state electronic properties of the van der waals transition metal trichalcogenide cops3. *Chemical Physics Letters* **823**, 140511 (2023).
- [30] Brec, R., Schleich, D., Ouvrard, G., Louisy, A. & Rouxel, J. Physical properties of lithium intercalation compounds of the layered transition-metal chalcogenophosphites. *Inorganic Chemistry* **18**, 1814–1818 (1979).
- [31] Jenjeti, R. N., Austeria, M. P. & Sampath, S. Alternate to molybdenum disulfide: A 2d, few-layer transition-metal thiophosphate and its hydrogen evolution reaction activity over a wide pH range. *ChemElectroChem* **3**, 1392–1399 (2016).
- [32] Hohenberg, P. & Kohn, W. Inhomogeneous electron gas. *Physical review* **136**, B864 (1964).

- [33] Kohn, W. & Sham, L. J. Self-consistent equations including exchange and correlation effects. *Phys. Rev.* **140**, A1133–A1138 (1965).
- [34] Dudarev, S. L., Botton, G. A., Savrasov, S. Y., Humphreys, C. J. & Sutton, A. P. Electron-energy-loss spectra and the structural stability of nickel oxide: an lsd+u study. *Physical Review B* **57**, 1505–1509 (1998). URL <http://dx.doi.org/10.1103/PhysRevB.57.1505>.
- [35] Kresse, G. & Hafner, J. Ab initio molecular dynamics for liquid metals. *Physical Review B* **47**, 558–561 (1993). URL <http://dx.doi.org/10.1103/PhysRevB.47.558>.
- [36] Kresse, G. & Furthmüller, J. Efficiency of ab-initio total energy calculations for metals and semiconductors using a plane-wave basis set. *Computational Materials Science* **6**, 15–50 (1996). URL [http://dx.doi.org/10.1016/0927-0256\(96\)00008-0](http://dx.doi.org/10.1016/0927-0256(96)00008-0).
- [37] Blöchl, P. E. Projector augmented-wave method. *Physical Review B* **50**, 17953–17979 (1994). URL <http://dx.doi.org/10.1103/PhysRevB.50.17953>.
- [38] Kresse, G. & Joubert, D. From ultrasoft pseudopotentials to the projector augmented-wave method. *Physical Review B* **59**, 1758–1775 (1999). URL <http://dx.doi.org/10.1103/PhysRevB.59.1758>.
- [39] Kresse, G. & Furthmüller, J. Efficient iterative schemes for ab initio total-energy calculations using a plane-wave basis set. *Phys. Rev. B* **54**, 11169–11186 (1996). URL <https://link.aps.org/doi/10.1103/PhysRevB.54.11169>.
- [40] Perdew, J. P., Burke, K. & Ernzerhof, M. Generalized gradient approximation made simple. *Physical Review Letters* **77**, 3865–3868 (1996). URL <http://dx.doi.org/10.1103/PhysRevLett.77.3865>.
- [41] Wang, V., Xu, N., Liu, J.-C., Tang, G. & Geng, W.-T. Vaspkit: A user-friendly interface facilitating high-throughput computing and analysis using vasp code. *Computer Physics Communications* **267**, 108033 (2021). URL <http://dx.doi.org/10.1016/j.cpc.2021.108033>.
- [42] Grimme, S., Antony, J., Ehrlich, S. & Krieg, H. A consistent and accurate ab initio parametrization of density functional dispersion correction (DFT-D) for the 94 elements H-Pu. *The Journal of Chemical Physics* **132**, 154104 (2010). URL <https://doi.org/10.1063/1.3382344>. https://pubs.aip.org/aip/jcp/article-pdf/doi/10.1063/1.3382344/15684000/154104_1_online.pdf.
- [43] Khumalo, F. & Hughes, H. Reflectance spectra of some fep s 3-type layer compounds in the vacuum ultraviolet. *Physical Review B* **23**, 5375 (1981).
- [44] Qi, B., Zhang, L. & Ge, L. Defect states emerging from a non-hermitian flatband of photonic zero modes. *Physical review letters* **120**, 093901 (2018).
- [45] Tong, Y., Chen, P., Chen, L. & Cui, X. Dual vacancies confined in nickel phosphosulfide nanosheets enabling robust overall water splitting. *ChemSusChem* **14**, 2576–2584 (2021).
- [46] Zhang, S. *et al.* Boosted photoreforming of plastic waste via defect-rich nips3 nanosheets. *Journal of the American Chemical Society* **145**, 6410–6419 (2023).

- [47] Wu, Z. *et al.* Adsorption of water molecules on pristine and defective nix₃ (x: S, se) monolayers. *Advanced Theory and Simulations* **4**, 2100182 (2021).
- [48] Wang, F. *et al.* New frontiers on van der waals layered metal phosphorous trichalco-
genides. *Advanced Functional Materials* **28**, 1802151 (2018).

Figures

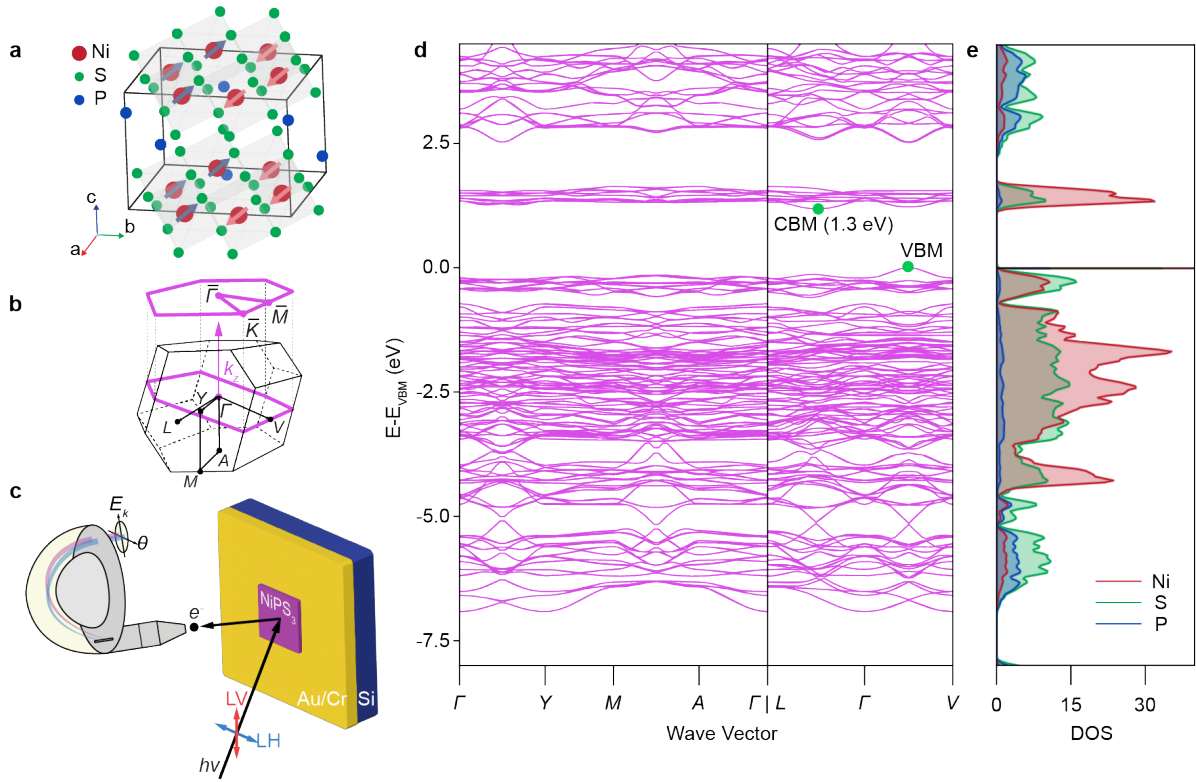


Figure 1: (a) Crystal and magnetic structure of NiPS₃⁴⁸. Blue and pink arrows stand for spin-up and spin-down in its antiferromagnetic state. (b) Three-dimensional Brillouin zone (BZ) with arrow indicate the direction of k_z . Hexagon on the top is the projection of the surface BZ. (c) Stratified arrangement of the NiPS₃ flakes on coated Si substrate and beam geometry with LH and LV stands for linear horizontal and linear vertical polarizations, respectively. (d) DFT calculated electronic structure of bulk NiPS₃ along all high-symmetry points and (e) the integrated density of states (DOS) with Ni, S, and P indicated by red, green, and blue, respectively. Conduction band minimum (CBM) and VBM are labeled with green dots.

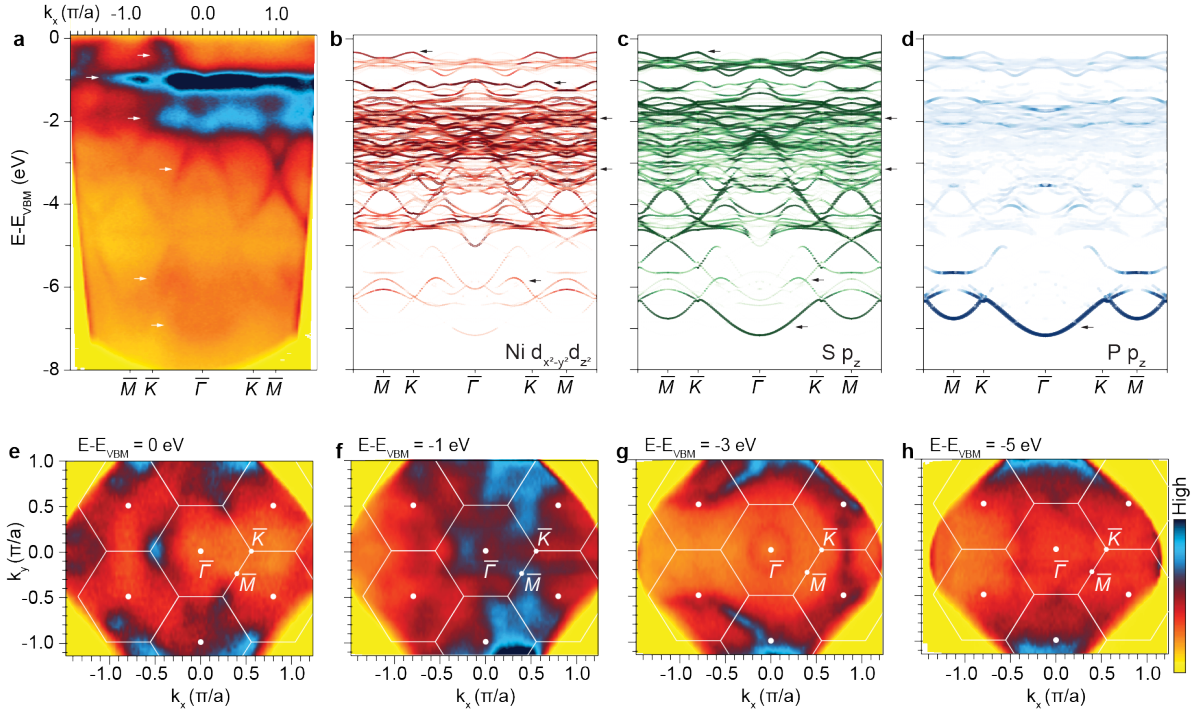


Figure 2: (a) Measured dispersion along the $\overline{MK\Gamma KM}$ direction at 6 K with LH beam at $h\nu = 126$ eV. The white arrows indicate the positions of the observed energy bands. (b)-(d) Band structure obtained with DFT+U approach ($U=2.0$ eV). The main contributing atomic orbitals are plotted, including the $d_{x^2-y^2}$ and d_{z^2} of Ni and p_z of S and P. The electronic states of different elements are distinguished by color: red, green, and blue represent Ni, S, and P, respectively. The intensity of the color indicates the band weight. The black arrows correspond to the white arrows in (a), indicating the primary contribution of different atomic orbitals to the experimentally obtained energy bands. (e)-(h) Constant energy maps at $E - E_{VBM} = 0$ eV, -1 eV, -3 eV, and -5 eV, with surface BZ boundaries labeled by white lines.

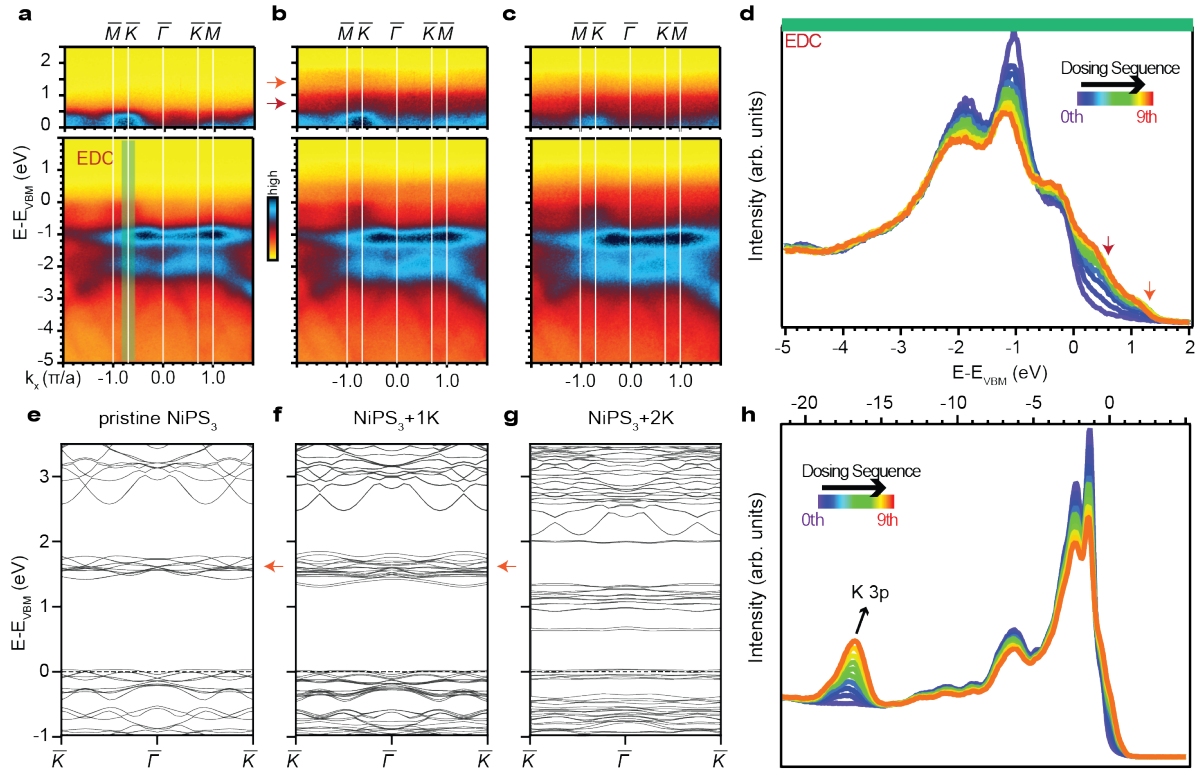


Figure 3: Dosing measurements. (a)-(c) ARPES data with (a) pristine sample before dosing, (b) dosing for 5 rounds, and (c) dosing for 9 rounds along the $\bar{M}\bar{K}\bar{\Gamma}\bar{K}\bar{M}$ direction. The dosing measurements were taken at 7 K with same LH beam at $h\nu = 126$ eV. The above images show an enlarged view of the CB region, with red and orange arrows representing the two newly appeared bands after dosing. (d) Energy distribution curve (EDC) at the \bar{K} point as indicated by the green line in (a), with color bar shows the dosing sequence. The arrows indicate the positions of the newly appeared bands in (b). (e)-(g) Calculated CB structure with DFT+U approach ($U=2.0$ eV) for (e) pristine NiPS₃, (f) NiPS₃ monolayer with 1 K atom per site, and (g) NiPS₃ monolayer with 2 K atoms per site. (h) Core level spectra for the dosing measurements.

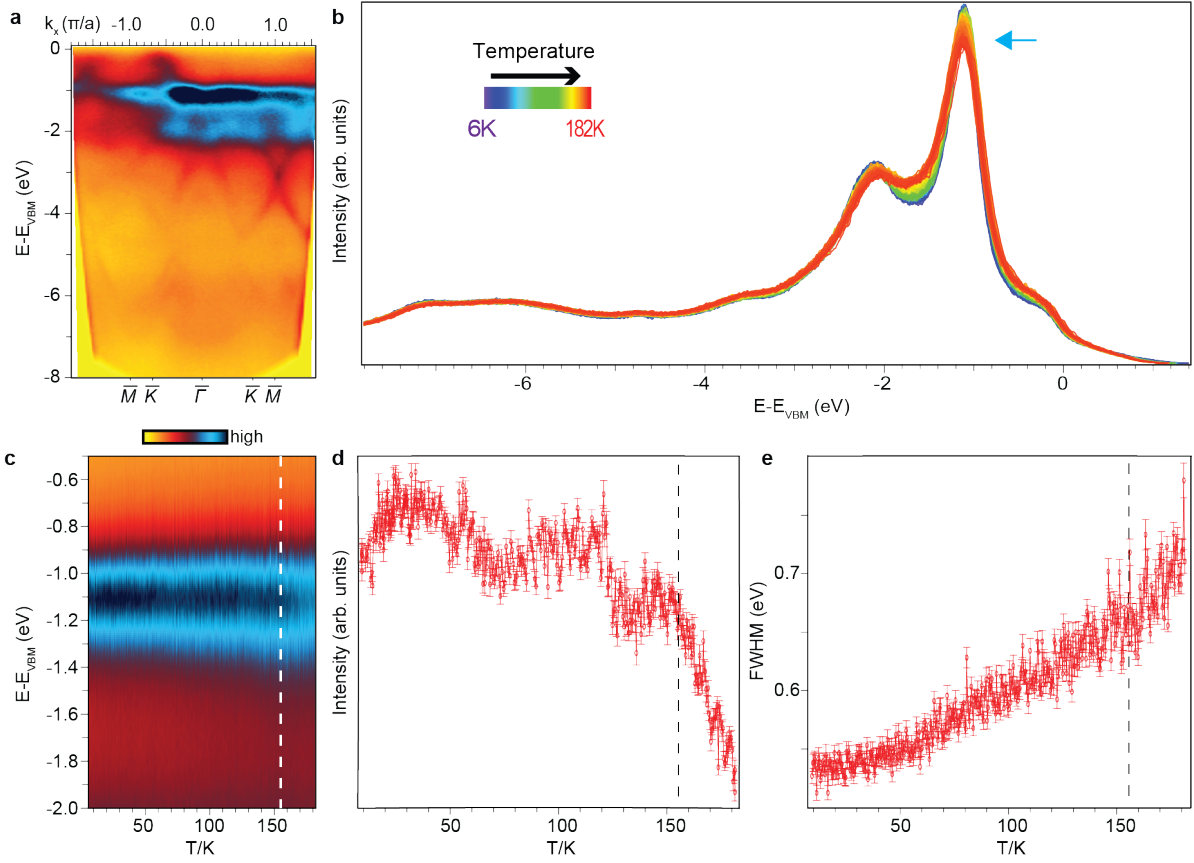


Figure 4: Temperature dependent measurements. (a) Measured dispersion under the same conditions as in Fig. 2(a), but at a temperature of 182 K in the paramagnetic state of NiPS₃. (b) Core level spectra during the temperature ramping from 6 K to 182 K with color bar indicate temperature. (c)-(e) The temperature dependent behaviors of the highest intensity band around $E - E_{VBM} = -1$ eV indicated by blue arrow in (b) with (c) shape of band, (d) peak intensity, and (e) full width at half maximum (FWHM). The dashed lines represent the T_N of NiPS₃.